agronomy

MDPI

Article

Algorithm for Locating Apical Meristematic Tissue of Weeds Based on YOLO Instance Segmentation

Daode Zhang, Rui Lu *, Zhe Guo, Zhiyong Yang, Siqi Wang and Xinyu Hu

School of Mechanical Engineering, Hubei University of Technology, Wuhan 430068, China
* Correspondence: lurui@hbut.edu.cn

Abstract: Laser technology can be used to control weeds by irradiating the apical meristematic tissue (AMT) of weeds when they are still seedlings. Two factors are necessary for the successful large-scale implementation of this technique: the ability to accurately identify the apical meristematic tissue and the effectiveness of the localization algorithm used in the process. Based on this, this study proposes a lightweight weed AMT localization algorithm based on YOLO (look only once) instance segmentation. The YOLOv8n-seg network undergoes a lightweight design enhancement by integrating the FasterNet lightweight network as its backbone, resulting in the F-YOLOv8n-seg model. This modification effectively reduces the number of parameters and computational demands during the convolution process, thereby achieving a more efficient model. Subsequently, F-YOLOv8n-seg is combined with the connected domain analysis algorithm (CDA), yielding the F-YOLOv8n-seg-CDA model. This integration enables the precise localization of the AMT of weeds by calculating the center-of-mass coordinates of the connected domains. The experimental results indicate that the optimized model significantly outperforms the original model; the optimized model reduces floating-point computations by 26.7% and the model size by 38.2%. In particular, the floating-point calculation is decreased to 8.9 GFLOPs, and the model size is lowered to 4.2 MB. Comparing this improved model against YOLOv5s-seg and YOLOv10n-seg, it is lighter. Furthermore, it exhibits exceptional segmentation accuracy, with a 97.2% accuracy rate. Experimental tests conducted on five different weed species demonstrated that F-YOLOv8n-seg-CDA exhibits strong generalization capabilities. The combined accuracy of the algorithm for detecting these weeds was 81%. Notably, dicotyledonous weeds were detected with up to 94%. Additionally, the algorithm achieved an average inference speed of 82.9 frames per second. These results indicate that the algorithm is suitable for the real-time detection of apical meristematic tissues across multiple weed species. Furthermore, the experimental results demonstrated the impact of distinctive variations in weed morphology on identifying the location of the AMT of weeds. It was discovered that dicotyledonous and monocotyledonous weeds differed significantly in terms of the detection effect, with dicotyledonous weeds having significantly higher detection accuracy than monocotyledonous weeds. This discovery can offer novel insights and avenues for future investigation into the identification and location of the AMT of weeds.

Keywords: laser weeding; apical meristematic tissue; instance segmentation; YOLOv8; connected domain analysis

Citation: Zhang, D.; Lu, R.; Guo, Z.; Yang, Z.; Wang, S.; Hu, X. Algorithm for Locating Apical Meristematic Tissue of Weeds Based on YOLO Instance Segmentation. *Agronomy* **2024**, *14*, 2121. https://doi.org/10.3390/agronomy14092121

Academic Editor: Yuxing Han

Received: 22 August 2024
Revised: 11 September 2024
Accepted: 13 September 2024
Published: 18 September 2024

1. Introduction

A reduced arable area, limited water supplies, and disturbances from abiotic and biotic variables like severe weather [1], frost [2], plant diseases [3], pest infestations [4], and weed issues [5] are just a few of the difficulties facing global agriculture today. Weeds are one of these biological restrictions that harm agriculture the most [6]. They compete with crops for critical resources such as nutrients, sunlight, and growing space, which in turn leads to a severe decline in crop yield and quality [7,8]. Farmers currently primarily use chemical weed control methods, applying herbicides to crops in the early stages of growth [9]. However, heavy herbicide use can pollute soil and increase potential environmental risk, and weeds resistant to herbicides are emerging [10]; in order to cope with these challenges, a number of non-chemical methods of weed control have been developed, such as mechanized weed control [11–13], electroshock weed control [14], steam weeding [15], and flame weeding [16]. Among the various weeding methods, most techniques, except electric shock weeding, are primarily designed for inter-row operations. These methods are not suitable for managing weeds between individual plants. In contrast, electric shock weeding can effectively target inter-plant weeds. However, this method requires direct contact between the weeding tool and the weeds. This contact poses a significant risk, as the tool may also inadvertently touch the crops, leading to a high incidence of seedling injury.

A unique and environmentally friendly laser weeding technique has been put out in light of machine vision's quick advancements [17]. With its precise placement, high weeding effectiveness, and low seedling injury rate, laser weeding is a new physical weeding technique that doesn't require the use of chemicals for inter-plant weeding [18–20]. The position of laser irradiation on weeds directly affects the weeding effect. Heisel et al. [21] employed computer vision technology to direct a laser for effective weed control by cutting grass stems. However, accurately locating the position of grass stems can be challenging for certain weed species. This difficulty complicates the arrangement of vision equipment, limiting the effectiveness of the approach. By examining the impact of laser action on weeds' apical meristematic tissues (AMT), Solvejg K. Mathiassen [22] et al. and colleagues demonstrated that using laser technology on weeds' AMT is a successful physical weed control strategy. Marx et al. [23] identified that the successful large-scale application of laser weed control technology hinges on the precise irradiation of the AMT of weeds. Accurately locating and targeting this tissue enhances weeding efficiency and reduces laser energy consumption. Consequently, the precise identification of the AMT of weeds is a crucial initial step in the laser weeding process.

Upon closer examination, it was discovered that the majority of weed recognition technology currently in use for laser weeding is restricted to the general recognition of weeds. For example, Zhu et al. [24] used YOLOX for weed recognition, calculating the actual coordinates of the weed's center of mass using the triangular similarity theorem based on the recognized image's center point. This allowed for the realization of weed localization. Hussain et al. [25] demonstrated the effectiveness of YOLOv5 in an autonomous laser weeding robot. Their evaluation indicated that YOLOv5 offers superior recognition accuracy and enhanced real-time performance for this application. Qin et al. [26] established an intelligent weed detection and laser weeding system based on YOLOv7, which was used for weed recognition and then localized by a binocular vision camera. The above study proved that the target detection algorithm under the YOLO framework has good accuracy and real-time performance for the weed identification task. However, it does not delve into the identification and localization of the AMT of weeds.

The AMT is located in the center of the apical leaf buds, which can be located by solving the coordinates of the weed's center of mass. This process involves detecting the weed's contour. The instance segmentation technique within the YOLO framework effectively segments and labels each object in an image at the pixel level. This technique is notable for its rapid detection speed and real-time performance, making it particularly suitable for applications requiring real-time contour detection [27]. However, YOLO's instance segmentation model still suffers from having a large number of parameters and a complex model structure, making it challenging to deploy in resource-constrained agricultural environments [28]. To overcome this challenge, researchers have begun to work on exploring ways to reduce the computational burden of deep learning models in order to improve their operational efficiency on resource-limited devices. In this context, a series of lightweight networks have been proposed, such as the MobileNet family [29,30], the ShuffleNet family [31,32], the EfficientNet [33], and the FasterNet [34] networks. The proposal of these lightweight networks provides the possibility for deep learning models to achieve efficient and real-time detection tasks in resource-constrained environments.

Based on the above analysis, this study proposes an algorithm to localize the AMT of weeds by combining the lightweight instance segmentation model with image processing technology, which adopts FasterNet as the backbone network and combines it with the connected domain analysis algorithm to realize the fast and accurate localization of the AMT of weeds. The main contributions of the paper are as follows:

- To enhance the weed data resources in cornfields, we expanded the existing weed dataset by collecting images of bowl flowers and incorporating publicly available datasets. This expansion aims to support the future development of weed recognition technology.
- This study proposes a lightweight instance segmentation model, F-YOLOv8n-seg, utilizing FasterNet as its backbone network. The model aims to address key issues associated with instance segmentation, including excessive model parameters, high computational demands, and substantial memory usage due to large-weight files. By mitigating these challenges, F-YOLOv8n-seg offers a viable solution for deploying instance segmentation algorithms in agricultural environments.
- A weed apical meristematic tissue localization algorithm (F-YOLOv8n-seg-CDA) is proposed in order to address the challenge of accurately locating the position of the apical meristematic tissue of weeds in laser weeding technology. This algorithm combines the traditional image processing method with the instance segmentation model, making it both efficient and accurate in locating the position of the apical meristematic tissue of weeds.
- We revealed the effects of differences in the morphological characteristics of different weed types on locating the apical meristem of weeds and found that the detection accuracy of dicotyledonous weeds is significantly higher than that of monocotyledonous weeds, which provides a new idea and direction for locating and detecting the apical meristem of weeds in future laser weed control technology.

2. Materials and Methods

2.1. Dataset Preparation

Calystegia hederacea Wall belongs to perennial trailing herbs, as shown in Figure 1, mainly harming wheat, cotton, corn, etc. Its inclusion in the dataset can increase the breadth and diversity of the dataset and can reflect the actual situation of weeds in the field more comprehensively. In addition, the addition of *Calystegia hederacea* Wall can enrich the environmental factors considered in the training of the model, enabling the model to learn more features related to the environment, thus helping to improve the model's adaptability and generalization ability in different environments and making it more accurate and effective in practical applications.

This paper constructs an image dataset of the *Calystegia hederacea* Wall, comprising 248 original images. To enhance the performance, robustness, and generalization of deep learning models, various data augmentation techniques have been applied to these collected images, including brightness enhancement, cropping, rotation, and flipping. Table 1 outlines the parameter settings for the data augmentation techniques, while Figure 2 illustrates the results of the data augmentation. The dataset was effectively expanded to 980 sheets by data enhancement techniques. To further expand the diversity of the dataset, the self-constructed dataset in this paper was fused with the dataset collected by Jiang et al. from an actual corn field (https://github.com/zhangchuanyin/weed-datasets (accessed on 12 September 2024)) to form a new dataset. The dataset collected by Jiang et al. contained corn and four weed species (*Bluegrass*, *Chenopodium album*, *Cirsium setosum*, and *Sedge*), and the new dataset after the fusion had 6978 images.

Figure 1. Example of *Calystegia hederacea* Wall.

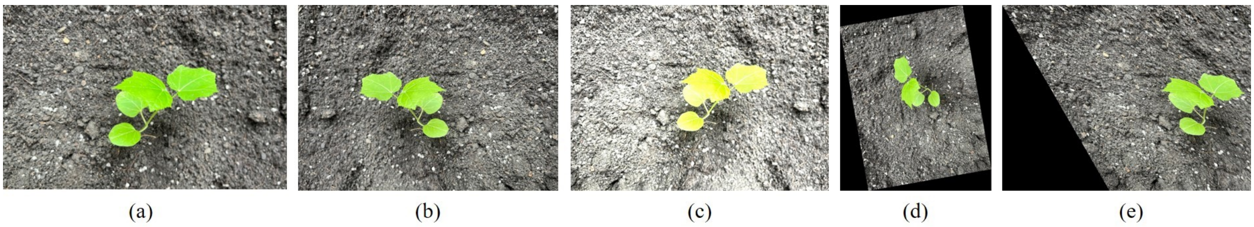

Figure 2. Example of data enhancement. (**a**) Original image. (**b**) Image flipped. (**c**) Brightness enhancement. (**d**) Arbitrary angle rotation. (**e**) Image cropping.

Table 1. Data enhancement technology parameter setting details.

Data Enhancement Type	Parameter Details	Image Example
Image flipped	Invert left and right	Figure 2b
Brightness enhancement	Brightness enhancement factor of 1.5	Figure 2c
Arbitrary angle rotation	Swivel range −180° to 180°	Figure 2d
Image cropping	Randomize the crop and set the cropped background to black	Figure 2e

This research focuses on the quality and details of the picture annotations in order to significantly enhance the model's recognition accuracy. All images were meticulously annotated using the Labelme tool to ensure accuracy and thus improve model learning. The choice of annotation technique includes the use of polygonal bounding boxes, which are well suited to capture the unique features of weeds, leading to a more accurate representation. As shown in Figure 3a, this type of annotation method reflects the thoroughness and accuracy of the entire process, demonstrating the comprehensiveness of the annotation. The file export format is JSON, and when training the model, the JSON file is converted to TXT format to adapt to the input requirements of the model. The YOLO instance segmentation model is able to segment the contours of weeds when applied to weed detection, which is crucial for the subsequent image processing and analysis work. Figure 3b shows an example of the model detection results, which visually presents the contours of the weeds, highlighting the model's power in the segmentation task.

(a) (b)

Figure 3. Examples of image annotation and model training results: (**a**) example of Labelme manual annotation; (**b**) example of model training results.

2.2. Test Platform

Table 2 displays the hardware and software settings utilized for training and testing the models. In the middle of constructing the model and performing training, the dataset is reasonably partitioned, where the training set is 80% of the data for model learning and optimization, and the validation set is 20% for evaluating the performance of the model during the training process. To guarantee the model's performance and the efficacy of training, the following model parameter choices were made: the training rounds were fixed at 100 to guarantee that the model would completely learn the features in the dataset and to ensure that the model would converge; the batch size was set at 16 to balance the training speed and memory efficiency; the initial value of the learning rate was set to 0.001, which can provide a sufficient update amplitude for the model in the early stage of training while avoiding oscillations in the later stage of training; and the rest of the parameters were adopted as the default settings of the model.

Table 2. Hardware and software environments.

Configuration	Parameter
Operation System	Windows 10 Professional Edition
CPU	12th Gen Intel(R) Core(TM) i7-12700F
GPUs	NVIDIA GeForce RTX 4060
Python	3.9.19
Pytorch	2.2.2
Cuda	12.1.0
Cudnn	9.1.1
Anaconda	24.3.0
Data Annotation Tools	Labelme

3. Algorithm for Locating the Apical Meristem of Weeds

The AMT is the core area of their growth and development, and it is the part of the plant that undergoes the most vigorous cell division and is capable of constantly undergoing cell division and increasing the number of cells in the growth zone, thus promoting plant growth. Illuminating this area with laser technology can effectively inhibit weed growth or kill weeds when they are young. The apical meristematic tissue is usually located in the center of the apical leaf bud, as shown in Figure 4, which is marked with a red circle, and its exact location can be located by the morphology of the grass leaf. Thus, localizing the AMT position requires obtaining the contour information of weeds, and the YOLO instance segmentation algorithm combines the rapidity of target detection with the accuracy of instance segmentation, which is particularly suitable for the contour detection of weeds.

Figure 4. Example of the location of apical meristematic tissues in different weed species.

3.1. F-YOLOv8n-Seg Instance Segmentation

The YOLOv8 instance segmentation model was chosen as the primary research model for this project due to the analysis presented above. This model's architecture consists of three main components: the backbone network, the feature fusion neck, and the segmentation head. The backbone network is responsible for extracting features from the input image and consists of the Conv (Convolutional Layer), C2f (Feature Fusion Convolution), and SPPF (Spatial Pyramid Pooling-Fast) layers. The feature fusion neck consists of FPN (Feature Pyramid), C2f (Feature Fusion Convolution) and Upsample. As shown in Figure 5, the architecture of YOLOv8 instance segmentation and its functional connections among each other are clearly demonstrated. C1–C5 in the figure represent different levels of feature maps, which are extracted from different stages of the model, and each stage corresponds to different scales and semantic information; e.g., the feature map at a lower level (C1) provides rich detail information and is suitable for the segmentation of small objects, while the feature map at a higher level (such as C5) provides rich semantic information and is suitable for segmentation of large objects. In the figure, P5, P4, and P3 denote different layers of different output layers in the model, which are designed to capture feature information at different scales for better detection of targets of different sizes. The YOLOv8 approach is built upon the YOLCAT framework. The architecture of YOLOv8 instance segmentation and its functional connections with each other are clearly shown in Figure 5. The YOLOv8 instance segmentation model provides several training models of different sizes, including n, s, m, l, and x versions, which trade off speed and accuracy, with a consequent increase in model complexity. In this paper, we aim to study the lightweight model, so we choose the lightest of all versions, the n version, called YOLOv8n-seg.

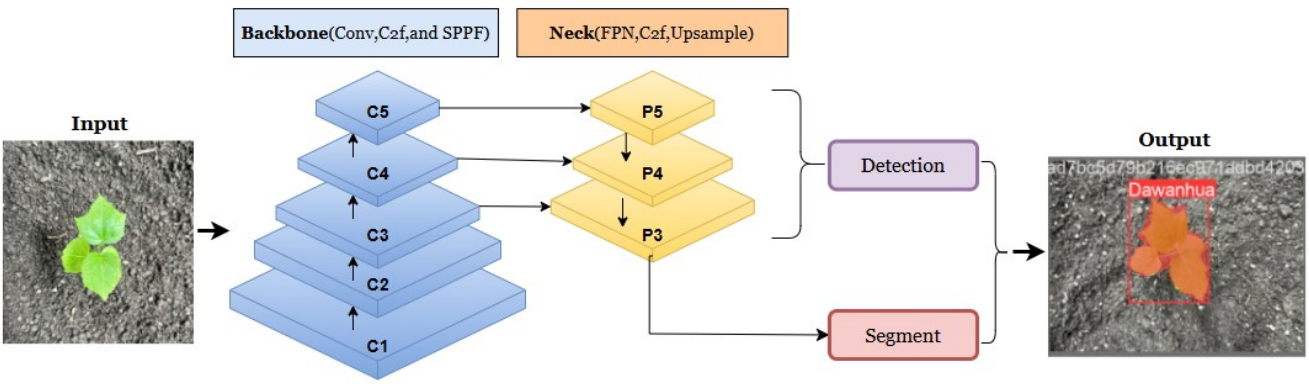

Figure 5. YOLOv8n-seg simple architecture diagram.

Although YOLOv8n-seg is the lightest of all versions, it still suffers from the problems of a high number of model parameters and high computational effort. To address the above problems, this study proposes to replace the backbone network of YOLOv8n-seg with a lightweight FasterNet network, and the optimized network structure is shown in Figure 6. A new partially convolved Pconv is proposed in FasterNet [34], which, as shown in the upper-right part of Figure 6, applies the regular Conv to only a portion of the input channel for spatial feature extraction and keep the rest of the channels unchanged, this method can effectively reduce the computational redundancy and memory access and effectively improve the computing speed while ensuring better detection accuracy. The integration of YOLOv8n-seg with FasterNet, resulting in F-YOLOv8n-seg, offers significant advantages. This combination leverages the efficient and high-precision detection capabilities of YOLOv8n-seg. Additionally, it optimizes model deployment in agricultural environments. The lightweight design of FasterNet reduces the model size and enhances computational speed, making it more suitable for practical applications in agriculture.

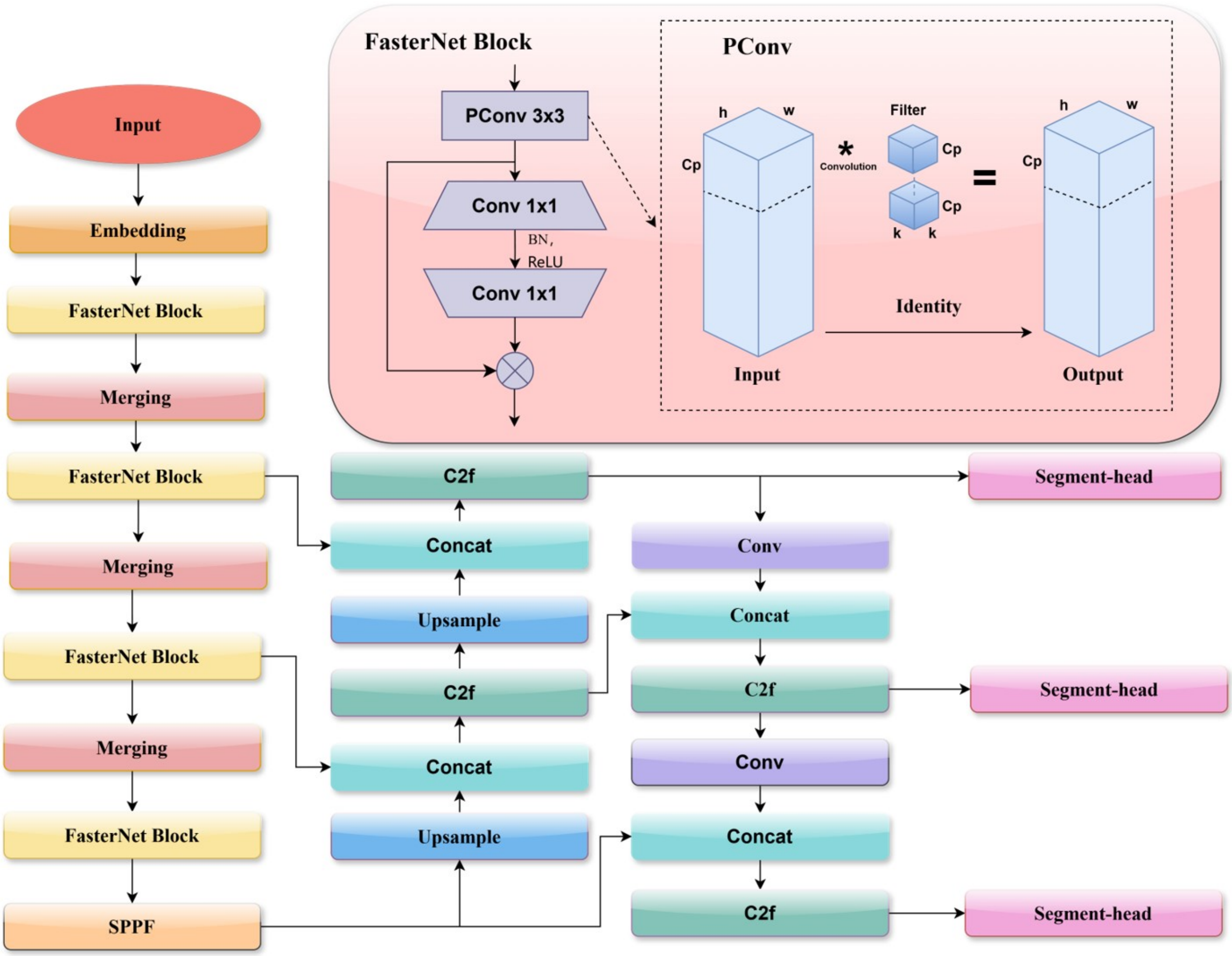

Figure 6. F-YOLOv8n-seg network structure diagram.

Combining the F-YOLOv8n-seg model with the connected domain analysis algorithm can give full play to the advantages of F-YOLOv8n-seg in image segmentation while using the connected domain algorithm to further process the segmentation results, which can efficiently and accurately achieve the positional localization of the AMT of weeds.

3.1.1. Connected Domain Analysis (CDA)

The connected domain is a fundamental concept in the field of image processing and computer vision [35,36]. In image processing, a connected domain refers to a region consisting of a collection of pixels with the same pixel value and adjacent positions. The purpose of the connected domain analysis (CDA) is to identify and mark these independent connected regions in an image, and then obtain the relevant image feature information such as the area, bounding box, and center of mass of these regions, which is widely used in many fields such as medicine [37–39], automated surveillance systems [40–42], and face recognition [43].

Connectivity domain analysis is usually concerned with the continuity and adjacency of pixel values, and in order to prevent the effect of fluctuating pixel values on the extraction of different connectivity domains, it is often applied to binarized images, i.e., containing only two-pixel values (e.g., 0 and 1). In binary images, a connected domain usually contains only one-pixel value, and to keep the discussion general, the starting pixel coordinates are denoted by $T(x,y)$ in a binary image of $W \times H$ pixel size, where $0 \leq x \leq W-1$, $0 \leq y \leq H-1$, and when applying this to weed detection, the background pixel value and crop pixel value are set to 0, and the weed pixel value is set to 1.

In image processing, pixels with the same value that are adjacent to each other form a connected domain, and each connected domain represents a separate object in the image. The connectivity domain is divided into 4-connectivity (horizontal and vertical adjacency) and 8-connectivity (horizontal, vertical and diagonal adjacency), as shown in Figure 7; 4-connectivity means that a pixel is adjacent to only four pixels directly above, below, left, and right of it, and 8-connectivity means that a pixel is adjacent to eight pixels around it, and these two different adjacencies make the connectivity domain different in shape and size. Specifically, 4-connectivity is more suitable for segmenting objects with clear edges and regular shapes. Since only horizontal and vertical connections are considered, when there are diagonal connections in the region, it will result in the region being segmented into several smaller quadruple connectivity regions, which is unsuitable for segmentation in complex environments.

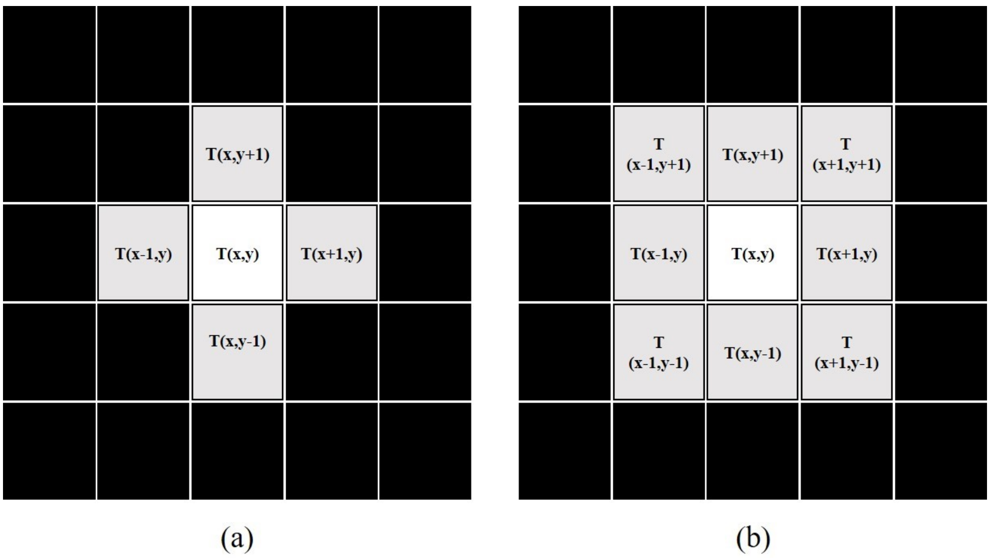

Figure 7. Pixel neighborhood: (**a**) 4-connected. (**b**) 8-connected.

The flow of the connectivity domain algorithm is shown in Figure 8, in connectivity domain analysis, the algorithm traverses each pixel of the image, detects its connectivity with its neighboring pixels, groups the pixels into different connectivity domains according to the type of connectivity, and assigns a unique identifier to each connectivity domain for subsequent processing and analysis. The connected domain analysis algorithm allows all foreground regions (weed regions) in an image to be labeled and a unique label to be assigned to each connected domain. The coordinates of the center of mass of the weed connectivity domains are then obtained to pinpoint the location of the apical meristematic tissue of the weed.

Connected domain analysis algorithm（CDA）

Input：
image：Segmented image to be labeled
label_value：Initial label value to distinguish between different connectivity domains

Output：
label_map：Tagged image where each connectivity domain is assigned a unique tag value

Steps:

1. Initialisation
    - Create a label_map of the same size as the image, with all elements initialised to 0
    - Create an empty stack for storing pixel coordinates
    - Initialise label_value=1
2. Scanning and labelling of connectivity domains
    - Scan each pixel in the image：
        - If image(x,y) is a foreground pixel and label_map(x,y)==0:
            - Label the current pixel: label_map(x,y) = label_value
            - Press (x, y) onto the stack
            - Call DFS (x, y) to depth-first search and label all pixels in the current connectivity field
            - Increment label_value to prepare a new label value for the next concatenated field
3. Depth-first search (DFS)
    - Call the DFS function:
        - If (x,y) is outside the image boundaries or label_map(x,y)! = 0, then return
        - Label the current pixel: label_map(x,y) = label_value
        - Iterate over the eight neighbouring pixel coordinates of (x, y)
4. Repeat step 2 until all pixels in the image have been traversed
5. Output label_map

Figure 8. Step-by-step diagram of the connectivity domain analysis algorithm.

3.1.2. Connected Domain Center-of-Mass Solver

The calculation of the connected domain center-of-mass is based on the concept of the geometric center, which is the equilibrium point of a shape or region. In image processing, the center of mass of a connected component can be calculated by mathematically averaging the positions of all the pixels within it. The center of mass is the weighted average of the coordinates of all the pixels within the connected domain, and the steps for calculating the center of mass are as follows:

Let m × n be the dimensional binary image $N(x, y)$, where the detected object is A, and the non-detected object is the background B; then, we have

$$N(x,y) = \begin{cases} 1((x,y) \in A) \\ 0((x,y) \in B) \end{cases} \quad (1)$$

The center of mass is defined as

$$Centroid_x = \frac{\sum_{(x,y)\in A} xN(x,y)}{\sum_{(x,y)\in B} N(x,y)} \tag{2}$$

$$Centroid_y = \frac{\sum_{(x,y)\in A} yN(x,y)}{\sum_{(x,y)\in B} N(x,y)} \tag{3}$$

where (x, y) is the pixel coordinate in the connectivity domain and N denotes the total number of pixels in the connectivity domain.

3.2. F-YOLOv8n-Seg-CDA

The F-YOLOv8n-seg-CDA algorithm presented in this paper seeks to accomplish the following goals: precisely identify and locate the apical meristematic tissues of weeds; optimize network resource occupation to enable the algorithm's better application to the agricultural environment; and provide critical technological support for the laser weed control technology. The specific implementation process of the algorithm is shown in Figure 9, where the input weed image is first processed using the F-YOLOv8n-seg model to quickly and accurately segment the weed region in the image and generate the weed mask with pixel-level accuracy. The generated weed mask is binarized, and the pixels in the mask are classified into two categories of weeds and non-weeds by setting a suitable threshold to reduce the pixel-value fluctuations on the connectivity domain analysis. The connectivity domain analysis algorithm is then applied to the binarized image to identify and mark the connectivity domains of all weeds. Finally, the center-of-mass coordinates were calculated for each identified connectivity domain, and the center-of-mass coordinates were used as the location of the apical meristem of the weed.

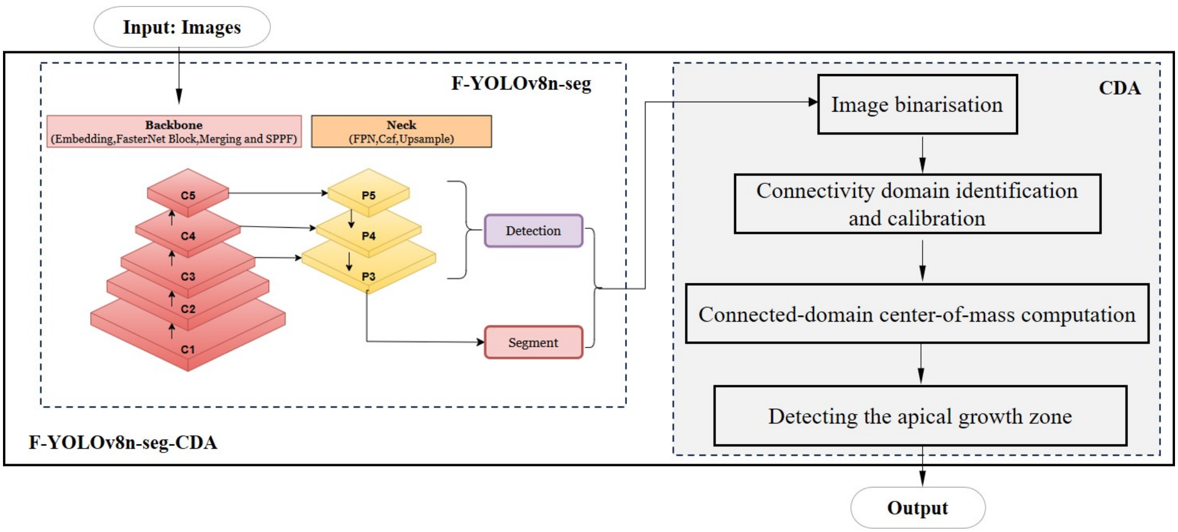

Figure 9. Flowchart of F-YOLOv8n-seg-CDA algorithm.

4. Results and Discussion

4.1. Evaluation Indicators

When assessing the effectiveness of instance segmentation algorithms, several crucial measures are frequently utilized, such as Mean Average Precision, Precision, and Recall. These metrics provide a comprehensive picture of the model's performance on the test data [44,45]. Among them, precision is used to measure the proportion of samples detected as positive that are truly positive (as shown in Equation (4)), recall indicates the proportion of all true objects that chants are correctly detected (as shown in Equation (5)), and mAP denotes the average of the mean accuracies of all categories.

$$Precision = \frac{TruePositives}{TruePositives + FalsePositives} \tag{4}$$

$$Recall = \frac{TruePositives}{TruePositives + FalseNegatives} \tag{5}$$

Typically, average precision (AP) for a single category is calculated by first ranking the results based on the confidence of the model predictions, subsequently plotting a curve of precision versus recall, and calculating the area under that curve, as shown in Equation (6).

$$AP = \int_0^1 Precision(Recall)d(Recall) \tag{6}$$

The mAP is calculated based on the mean of the precision at different recall levels and is usually associated with Intersection over Union (IoU). IoU is a measure of the degree of overlap between two regions, which is defined by calculating the ratio of intersection to concurrency of two regions. In this study, the goal was to identify two categories, so the mAP calculated was the average precision (AP) of the two categories, as calculated by Equation (7). Specifically, mAP@0.5 represents the AP value when the IoU (Intersection over Union) threshold is set at 0.5. Meanwhile, mAP@0.50:0.95 indicates the average of the AP values calculated at IoU thresholds incrementing from 0.5 to 0.95, increasing by 0.05 at each step. These AP values are then averaged according to Formula (5) to produce the final mAP@0.50:0.95 result.

$$IoU(A,B) = \frac{|A \cap B|}{|A \cup B|} \tag{7}$$

$$mAP = \frac{1}{n}\sum_{i=1}^{n} APi \tag{8}$$

$$mAP = \frac{AP_{IoU=0.5} + AP_{IoU=0.55} + \ldots + AP_{IoU=0.95}}{k} \tag{9}$$

In the formula, k refers to the number of IoU thresholds being considered.

The F1 score is a popular measure of performance for classification problems. It combines precision and recall and is presented as a harmonic mean, taking values between 0 and 1. Its calculation formula is as follows:

$$F1 - score = \frac{2 \times Precision \times Recall}{Precision + Recall} \tag{10}$$

4.2. Optimizer Selection

This study examines the impact of various optimizers on the model to ensure optimal performance. When processing the dataset, it was divided into two categories: weeds and maize, based on practical application scenarios, aiming to efficiently identify all types of weeds, as well as to ensure that maize plants can be correctly distinguished to avoid incorrectly determining the crop as a weed during the identification process.

Under uniform training hyperparameters and methodologies, three popular optimizers—SGD (stochastic gradient descent), Adam (adaptive moment estimation), and AdamW (Adam with weight decay)—are compared. Figure 10 illustrates the variations in the loss functions of different optimizers, where green represents SGD, blue denotes Adam, and orange indicates AdamW. It is evident from the graph that both Adam and AdamW outperform SGD in terms of the speed of the loss function reduction and overall performance, with AdamW slightly surpassing Adam. Figure 11 presents the performance of each optimizer concerning accuracy; the data indicate that AdamW demonstrates the best performance across all accuracy metrics. Based on these findings, this study selects AdamW as the optimization tool for model training to achieve optimal performance during the training process.

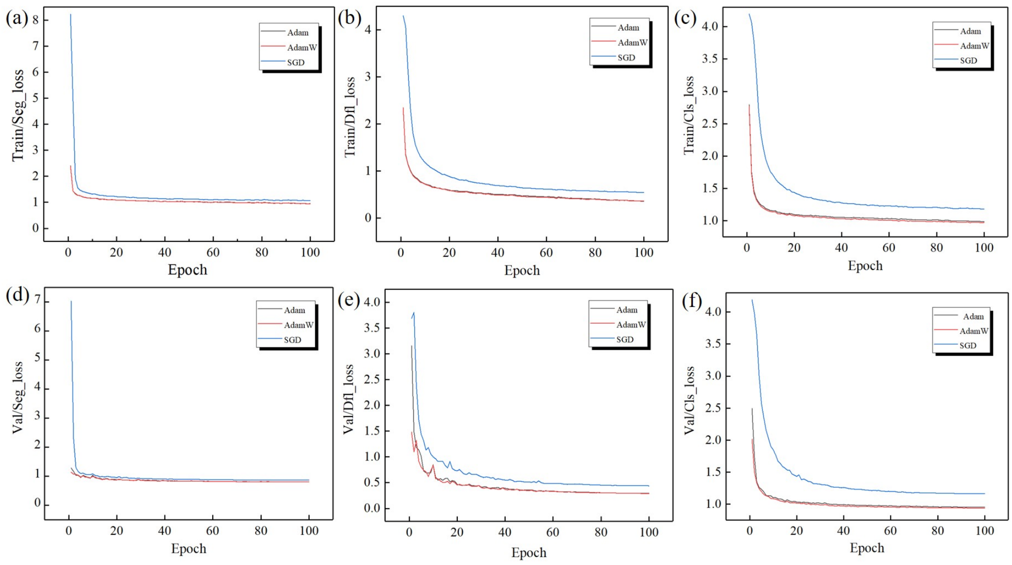

Figure 10. Comparison of loss variations: (**a**) Segmentation loss of the model training process; (**b**) directional feature loss of the model training process. (**c**) Classification loss of the model training process. (**d**) Segmentation loss of the prediction process. (**e**) Directional feature loss of the prediction process. (**f**) Classification loss of the prediction process.

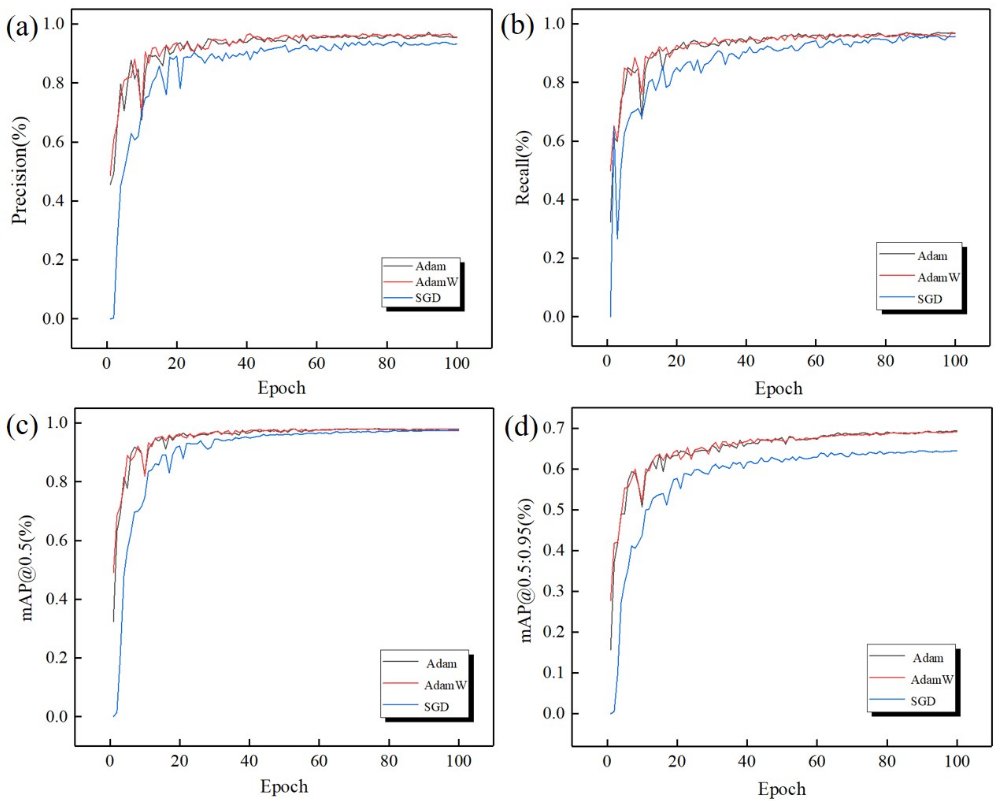

Figure 11. Comparison of change curves for evaluation metrics: (**a**) Comparison of precision. (**b**) Comparison of recall. (**c**) Comparison of mAP@0.5. (**d**) Comparison of mAP@0.5:0.95.

4.3. Comparison of Different Lightweight Networks

To validate the impact of different lightweight networks on the performance of the YOLOv8n-seg model, the backbone network of YOLOv8n-seg was reconstructed using four networks: MobileNetv3, ShuffleNetv2, FasterNet, and EfficientNet. From the results (Tables 3–5), the YOLOv8n-seg+ShuffleNetv2 (S2-YOLOv8n-seg) and YOLOv8n-seg+EfficientNet (E-YOLOv8n-seg) models demonstrate a reduction in model size of 38.2% and 32.4%, respectively, compared with the original model. The FLOPs decreased by 26.7% and 20.8%, while the number of parameters dropped by 39.8% and 20.1%. However, the comprehensive accuracy of these two models in detecting boxes decreased by 1.4% and 0.5%, and the comprehensive accuracy in segmentation marks decreased by 1.3% and 0.6%. YOLOv8n-seg+MobileNetv3 (M3-YOLOv8n-seg) and YOLOv8n-seg+FasterNet (F-YOLOv8n-seg) improved the combined accuracy of the models in the box by 0.5% and 0.4%, respectively, and in the Mark by 0.5% and 0.8%, respectively, compared with the original model, and compared to the M3-YOLOv8n-seg, the F- YOLOv8n-seg not only maintains a small increase in accuracy, but also achieves a better performance in model size and number of parameters. M3-YOLOv8n-seg reduces the model size by 19.1%, the number of parameters by 33.8%, and the amount of floating-point computation by 20% on the basis of the original model, whereas the model size, the number of parameters and the amount of floating-point computation were reduced by 38.2%, 25.8%, and 38.7%, respectively. Considering the model size, number of parameters, and accuracy performance, F-YOLOv8n-seg shows the best performance, and, therefore, FasterNet is finally chosen as the backbone network of the algorithm.

Table 3. Comparison of detection Box-related parameters for different lightweight networks.

Model	P/%	R/%	mAP@50	mAP@50-95
YOLOv8n-seg	96.5	96.4	98.2	84.7
+MobileNetv3	97.0	95.2	98.4	83.6
+ShuffleNetv2	95.1	95.2	97.7	82.5
+EfficientNet	96.0	96.8	98.3	84.1
+FasterNet	96.9	95.8	98.4	83.9

Table 4. Comparison of segmentation Mark-related parameters for different lightweight networks.

Model	P/%	R/%	mAP@50	mAP@50-95
YOLOv8n-seg	96.4	96.2	98.0	69.2
+MobileNetv3	96.9	95.1	98.1	68.1
+ShuffleNetv2	95.1	95.1	97.6	67.7
+EfficientNet	95.8	96.6	98.2	68.8
+FasterNet	97.2	95.9	98.4	68.9

Table 5. Comparison of the degree of model lightness.

Model	Parameters (Millions)	Model Size/MB	FLOPs/G
YOLOv8n-seg	3.264	6.8	12.0
+MobileNetv3	2.607	5.8	9.6
+ShuffleNetv2	1.966	4.2	8.8
+EfficientNet	2.162	5.5	9.5
+FasterNet	2.001	4.2	8.9

The training process changes for F-YOLOv8n-seg are illustrated in Figure 12. From the evaluation metric curves for Box and Mark shown in Figure 12a,b, it can be observed that during the early stages of training, the model's average precision, recall, and accuracy all increase rapidly, indicating that the model can quickly learn the key features that distinguish between weeds and corn in the initial phase. The loss change curves shown in Figure 12c,d reveal that as iterations progress, the loss values tend to stabilize. After 100 iterations, the loss values begin to stabilize, suggesting that the model does not exhibit significant overfitting or underfitting during the training process.

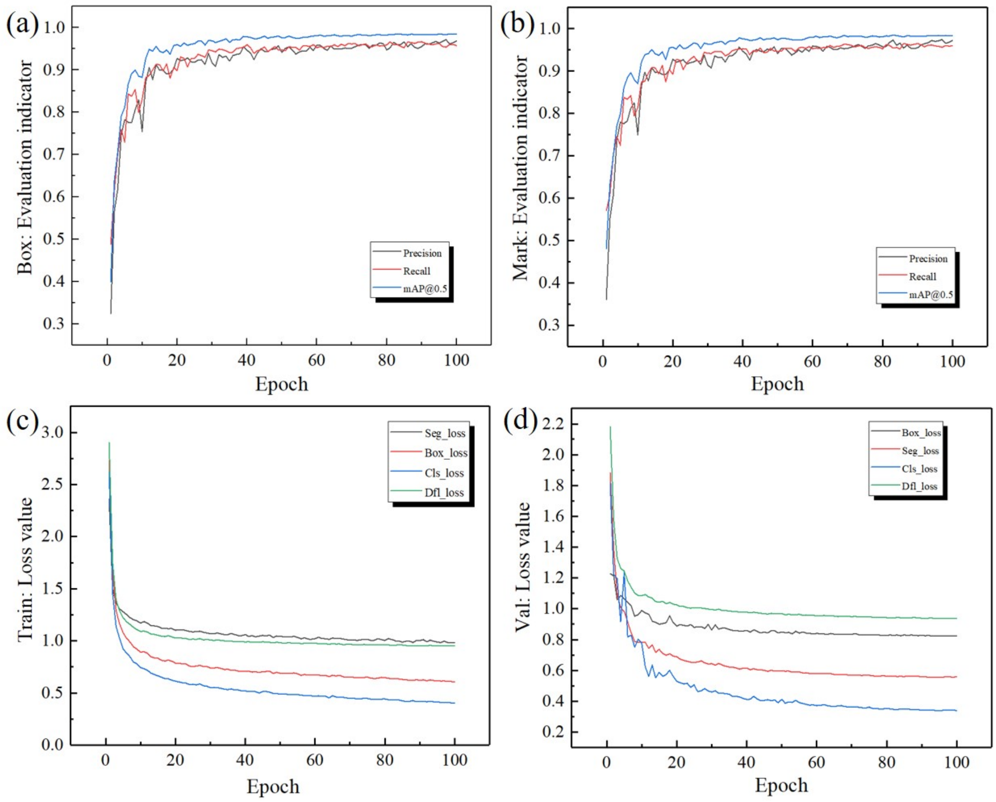

Figure 12. F-YOLOv8n-seg training process curves: (**a**) Evaluation metrics change curve for Box. (**b**) Evaluation index change curve of Mark. (**c**) Loss change curve of training process. (**d**) Loss change curve of prediction process.

4.4. Comparison with Other YOLO Algorithms

The state-of-the-art YOLOv10n-seg and YOLOv5s-seg algorithms were compared with the F-YOLOv8n-seg method to assess its performance more thoroughly. The analysis results indicate that F-YOLOv8n-seg surpasses YOLOv5s-seg and approaches the level of YOLOv10n-seg in terms of detection box performance parameters (Table 6). F-YOLOv8n-seg's detection accuracy is 96.9%, which is 0.2% higher than that of yolov5s-seg and 0.2% lower than that of YOLOv10n-seg. F-YOLOv8n-seg reaches the greatest level of 97.2% in the segmentation mask accuracy key metric (Table 7), and its accuracy is 0.3% and 1% greater than that of YOLOv10n-seg and YOLOv5s-seg, respectively. This indicates its strong competence in the instance segmentation task.

Table 6. Comparison of detection Box related parameters for each algorithm.

Model	P/%	R/%	mAP@50	mAP@50-95
YOLOv10n-seg	97.1	96.5	98.7	85.3
YOLOv5s-seg	96.4	95.8	98.2	84.5
F-YOLOv8n-seg	96.9	95.8	98.4	83.9

Table 7. Comparison of detection Mark related parameters for each algorithm.

Model	P/%	R/%	mAP@50	mAP@50-95
YOLOv10n-seg	96.9	96.3	98.6	70.0
YOLOv5s-seg	96.2	95.7	98.0	69.2
F-YOLOv8n-seg	97.2	95.9	98.4	68.9

One of the objectives of this study is to seek a method that can reduce the computational burden of the model while maintaining or even enhancing its accuracy. Although YOLOv10n-seg slightly surpasses F-YOLOv8n-seg in certain performance parameters related to detection and segmentation, F-YOLOv8n-seg outperforms YOLOv10n-seg in terms of model size, parameter count, and inference speed. As shown in Table 8, compared to YOLOv10n-seg, F-YOLOv8n-seg achieves a 30% reduction in model size, a 16.2% decrease in parameter count, a 15.2% reduction in FLOPs, and boasts a faster inference speed. Based on the above analysis, this study concludes that F-YOLOv8n-seg is more suitable to be deployed in agricultural environments with specific needs for model lightweight compared to YOLOv5s-seg and YOLOv10n-seg.

Table 8. Comparison of detection Mark related parameters for each algorithm.

Model	Parameters (Millions)	Model Size/MB	FLOPs/G	Forward Pass Time (ms)
YOLOv10n-seg	2.387	6.0	10.5	2.5
YOLOv5s-seg	2.761	5.8	11.0	3.6
F-YOLOv8n-seg	2.001	4.2	8.9	2.2

4.5. Evaluation of the F-YOLOv8n-Seg-CDA Algorithm

In an attempt to evaluate the generalization ability of the F-YOLOv8n-seg-CDA algorithm in identifying the apical growth zones of different weed species, 100 images were randomly selected from each of the five weed species to construct a test set containing 500 images dedicated to evaluating the performance of the proposed algorithm. As shown in Figure 12, the red dots indicate the location of the localized AMT, and as can be observed, the location of the AMT can be accurately localized regardless of the type of weed detected. The results confirm that the proposed algorithm has good generalization when dealing with diverse weed detection tasks, indicating that the algorithm can be effectively applied to the task of locating the apical meristematic tissues of multiple types of weeds.

In addition, the detection accuracy of F-YOLOv8n-seg-CDA was evaluated. Given that the context of this study is laser weed control technology, where one of the important evaluation metrics is the number of weeds removed, the performance of weed identification should also be evaluated based on the number of weeds identified.Specifically, if the image processing process is able to accurately identify the presence of multiple weeds in a single image, the count of successful identification should be increased by one unit equal to the number of weeds identified, rather than simply based on the entire image. Such an evaluation is more accurate than simply judging based on the entire image.The detection results in Table 9 show that the algorithm has a combined detection accuracy of 81.1% and an average inference speed of 82.9 frames/sec, which is a good performance in the field of weed AMT localization.However, the detection accuracy showed significant differences when targeting specific species of weed detection. Specifically, when detecting the dicotyledonous weeds *Chenopodium album*, *Cirsium setosum* and *Calystegia hederacea* Wall, the algorithm's detection accuracies were as high as 89%, 92% and 94%, respectively, indicating that the algorithm is highly accurate and reliable in locating the apical meristem of dicotyledonous weeds. In contrast, when detecting the monocotyledonous weeds bluegrass and sedge, its detection accuracy was lower, only 50% and 51%.

There were significant differences between dicotyledonous and monocotyledonous weeds in locating the position of their AMT, which was explained by the significant differences in leaf morphology between dicotyledonous and monocotyledonous weeds. Dicotyledonous weeds have broader leaves with more branches and slender and dense leaf veins, and these features make dicotyledonous weeds present a more symmetrical shape in the image, which is favorable for image recognition algorithms to capture their center of mass. The leaf morphology of monocotyledonous weeds is in the form of long strips or bands (e.g., the first and second rows of Figure 13), the length of the leaf blade is much larger than the width, the leaf blade is sparsely distributed and the leaf veins are underdeveloped, and this leaf morphology makes the monocotyledonous weeds present irregular shapes in the image, which increases the difficulty of the algorithm to accurately locate their center of mass. Since the center of the mass point is important for locating the position of the AMT of a weed, this challenge directly affects the accuracy performance of the algorithm on monocotyledonous weeds and, therefore, leads to the poor performance of the algorithm in detecting bluegrass and sedge. The results of this experiment reveal that differences in plant morphological features have a greater impact on the algorithm for locating the AMT of weeds based on image processing techniques.

Table 9. Localisation accuracy of apical meristematic tissue of five weed species.

Weed Type	Name	Number of Images	Number of Weeds	Correctly Identify the Number of Apical Growing Point	Recognition Accuracy (%)
Dicotyledon	*Chenopodium album*	100	112	100	89
	Cirsium setosum	100	110	101	92
	Calystegia hederacea Wall	100	403	379	94
Monocotyledon	Sedge	100	105	52	50
	Bluegrass	100	134	69	51

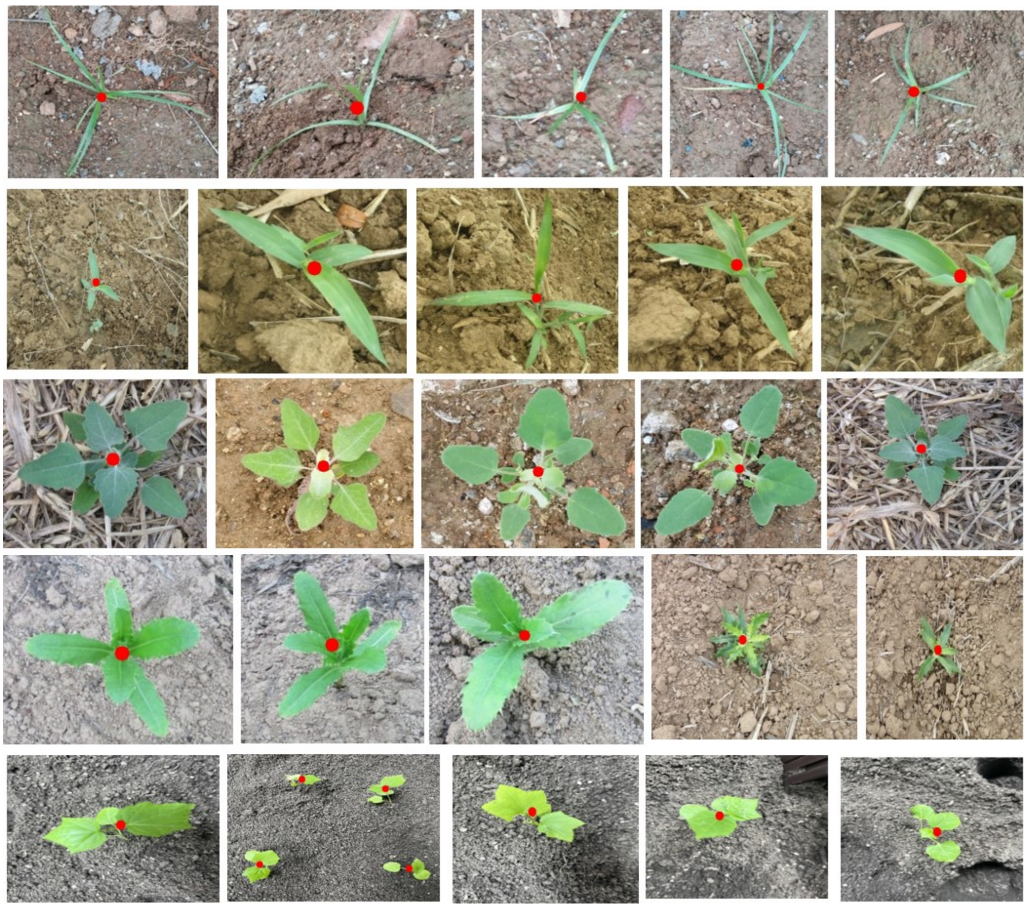

Figure 13. Localisation of apical meristematic tissue in five weed species.

The proposed algorithm was compared with recent research results on related topics, as shown in Table 10. Chen et al. [46] proposed to use deep migration learning for identifying common weeds in cotton fields, and the model can have an F1-Score value as high as 98%, but it has an average inference speed of only 3.0 FPS and a model size of 42.5 MB. Zhang et al. [45] designed a SE: YOLOv5x model specifically for identifying lettuce and weeds, which achieved an F1-Score of 97.3%, significantly exceeding that of a traditional support vector machine. Still, the model had many parameters and the model weights file reached 105.9 M. Peng et al. [47] proposed an improved RetinaNet model for weeds in rice fields, which had an average inference speed of 24.2 FPS and a model size of 24.33 MB. Zou et al. [48] proposed an improved UNet model for weed detection in wheat fields for segmentation of green bristlegrass in complex backgrounds, which had an F1 score and processing speed of 91.2% and 52 FPS, respectively. Hua et al. [49] proposed to use the improved YOLOv5s target detection algorithm to identify weeds, while the ultra-green features combined with the OTSU threshold segmentation algorithm to extract the foreground image of the identified weeds in the detection frame, as a way to achieve the identification of the apical meristematic tissue of weeds. The F1-Score, Model size and average inference speed of this algorithm are 96.9%, 8.08, and 37.2 FPS, respectively. In addition, Hu et al. [50] proposed a lightweight deep learning model for real-time lettuce identification and weed severity classification and applied it to a novel mechanical laser collaborative in-row weeding robot, which had a model size of 18.4 MB, an F1-Score of 95.7%, and an average inference speed of 37.3 FPS. The F1-Score of the F-YOLOv8n-seg-CDA algorithm is 94%, which is not the best value, but the algorithm has the smallest model and the fastest inference speed. The comparison further demonstrates that the F-YOLOv8n-seg-CDA algorithm has great potential for application in resource-limited environments.

Table 10. Comparison of findings in recent years.

Reference	Model	F1-Score (%)	Model Size (MB)	Average Processing Speed (FPS)
Chen et al. [46]	ResNet101	98.9	42.5	3.0
Zhang et al. [45]	SE: YOLOv5x	97.3	105.9	52.4
Peng et al. [47]	RetinaNet	—	24.3	24.2
Zou et al. [48]	UNet	91.2	—	52
Hua et al. [49]	Improved YOLOv5s	96.9	8.1	37.2
Rui Hu et al. [50]	Multimodule-YOLOv7-L	95.7	18.4	37.3
Proposed method	F-YOLOv8n-seg-CDA	94.0	4.2	82.9

5. Conclusions

Faced with the problem of the complexity and variety of weed species in cornfields and the scarcity of relevant datasets, this study first set out to expand the weed dataset, which was enriched by collecting images of bowl-busting flowers and integrating publicly available dataset resources. A lightweight instance segmentation model, F-YOLOv8n-seg, is proposed to address the high computational resource requirements of deep learning models in agricultural applications. The model replaces the backbone network with FasterNet to reduce the computational burden of the model. A novel method, F-YOLOv8n-seg-CDA, is suggested to overcome the difficulties encountered by laser weed control technology in precisely localizing the apical meristematic tissue of weeds. This method combines an enhanced YOLO instance segmentation model with a connected domain analysis algorithm.

The optimized F-YOLOv8n-seg model reduces the computational resource requirement without sacrificing the detection accuracy. Compared with the original model, its model size is reduced by 38.2% and the amount of parameters is reduced by 26.7%, while the detection accuracy is improved by 0.8%. Compared with similar state-of-the-art lightweight YOLO algorithms YOLOv10n-seg and YOLOv5s-seg, F-YOLOv8n-seg shows advantages in model size and parameter counts, with model size reduced by 30% and 27.6%, parameter counts reduced by 16.2% and 27.5%, and floating-point computation reduced by 15.2% and 19%, respectively. The accuracy of the segmentation mask is also improved by 0.8% and

1%, which proves that F-YOLOv8n-seg is more suitable to be applied in resource-limited agricultural environments.

The F-YOLOv8n-seg-CDA algorithm achieved a combined detection accuracy of 81% for the five weed species, with an average inference speed of 82.9 FPS. The algorithm performed well in the detection of dicotyledonous weeds, with detection accuracies as high as 89%, 92%, and 94%, respectively, for *Chenopodium album*, *Cirsium setosum*, and *Calystegia hederacea* Wall, While the detection accuracy of monocotyledonous weeds bluegrass, and sedge grass was lower, only 51% and 50%.

In conclusion, this paper's research offers a fresh approach to the problem of pinpointing weeds' apical meristematic tissue location in laser weeding systems. The suggested algorithm is more appropriate for the agricultural automation application situation due to the study's lightweight model improvement. An innovative method for identifying and locating the apical meristematic tissues of weeds is shown by revealing the impact of feature changes in weed morphology on the algorithm for finding the apical meristematic tissues of weeds based on image processing techniques.

In future research, more attention will be paid to the leaf morphology characteristics of monocotyledonous weeds to further improve the algorithm's ability to locate the position of the apical meristematic tissues of such weeds, with a view to achieving higher overall detection accuracy. In addition, in the next research, we will further expand the weed dataset to enhance the generalisation ability of the model and aim to effectively apply the model to real field environments, contributing more to the development of laser weed control technology.

Author Contributions: Conceptualization, D.Z. and R.L.; methodology, R.L.; investigation, R.L. and Z.G.; data curation, R.L., S.W. and Z.G.; writing—original draft preparation, D.Z. and R.L.; writing—review and editing, D.Z., R.L. and Z.Y.; funding acquisition, D.Z. and X.H. All authors have read and agreed to the published version of the manuscript.

Funding: This study was supported by the National Natural Science Foundation of China (No. 52075152) and the Innovative Group Program of Hubei Province (No. 2023AFA037).

Data Availability Statement: The data presented in this study are available on request from the corresponding authors.

Acknowledgments: We would also like to thank all reviewers for their valuable comments and Xuehui Liang for providing technical guidance for this paper.

Conflicts of Interest: The authors declare no conflicts of interest.

References

1. Raj, E.F.I.; Appadurai, M.; Athiappan, K. Precision farming in modern agriculture. In *Smart Agriculture Automation Using Advanced Technologies: Data Analytics and Machine Learning, Cloud Architecture, Automation and IoT*; Springer: Berlin/Heidelberg, Germany, 2022; pp. 61–87.
2. Shammi, S.; Sohel, F.; Diepeveen, D.; Zander, S.; Jones, M.G.; Bekuma, A.; Biddulph, B. Machine learning-based detection of freezing events using infrared thermography. *Comput. Electron. Agric.* **2022**, *198*, 107013. [CrossRef]
3. Haque, M.R.; Sohel, F. Deep network with score level fusion and inference-based transfer learning to recognize leaf blight and fruit rot diseases of eggplant. *Agriculture* **2022**, *12*, 1160. [CrossRef]
4. Amrani, A.; Sohel, F.; Diepeveen, D.; Murray, D.; Jones, M.G. Insect detection from imagery using YOLOv3-based adaptive feature fusion convolution network. *Crop. Pasture Sci.* **2022**, *74*, 615–627. [CrossRef]
5. Liu, J.; Xiang, J.; Jin, Y.; Liu, R.; Yan, J.; Wang, L. Boost precision agriculture with unmanned aerial vehicle remote sensing and edge intelligence: A survey. *Remote Sens.* **2021**, *13*, 4387. [CrossRef]
6. Little, N.G.; DiTommaso, A.; Westbrook, A.S.; Ketterings, Q.M.; Mohler, C.L. Effects of fertility amendments on weed growth and weed–crop competition: A review. *Weed Sci.* **2021**, *69*, 132–146. [CrossRef]
7. Patel, D.; Kumbhar, B. Weed and its management: A major threats to crop economy. *J. Pharm. Sci. Biosci. Res.* **2016**, *6*, 453–758.
8. Iqbal, N.; Manalil, S.; Chauhan, B.S.; Adkins, S.W. Investigation of alternate herbicides for effective weed management in glyphosate-tolerant cotton. *Arch. Agron. Soil Sci.* **2019**, *65*, 1885–1899. [CrossRef]
9. Harker, K.N.; O'Donovan, J.T. Recent weed control, weed management, and integrated weed management. *Weed Technol.* **2013**, *27*, 1–11. [CrossRef]
10. Heap, I. *Herbicide Resistant Weeds*; Springer: Berlin/Heidelberg, Germany, 2014.

11. Niu, M.; Fang, H.; Jian, S. Research on design and operation performance of maize hoe type weeder. *Agric. Equip. Veh. Eng.* **2022**, *60*, 6–9.
12. Hu, L.; Luo, X.; Yan, Y.; Chen, X.; Zen, S.; Zhang, L. Development and experiment of intra-row mechanical weeding device based on trochoid motion of claw tooth. *Trans. Chin. Soc. Agric. Eng.* **2012**, *28*, 10–16.
13. Ma, X.; Yang, Y.; Wang, Z. The consumption reduction and experiment conducted on tillage parts of the rotary mower. *J. Agric. Mech. Res.* **2022**, *44*, 94–98.
14. Slaven, M.J.; Koch, M.; Borger, C.P. Exploring the potential of electric weed control: A review. *Weed Sci.* **2023**, *71*, 403–421. [CrossRef]
15. Bitarafan, Z.; Kaczmarek-Derda, W.; Berge, T.W.; Tørresen, K.S.; Fløistad, I.S. Soil steaming to disinfect barnyardgrass-infested soil masses. *Weed Technol.* **2022**, *36*, 177–185. [CrossRef]
16. Rask, A.; Andreasen, C.; Kristoffersen, P. Response of Lolium perenne to repeated flame treatments with various doses of propane. *Weed Res.* **2012**, *52*, 131–139. [CrossRef]
17. Bayramian, A.; Fay, P.; Dyer, W. Weed control using carbon dioxide lasers. In Proceedings of the Western Society of Weed Science, Salt Lake City, UT, USA, 10–12 March 1992.
18. Christensen, S.; Heisel, T.; Schou, J. Severing or Damaging Apparatus for Unwanted Plants Comprises an Optical Recognition System That Differentiates between Different Types of Plants with a Light Generating Source to Expose the Plant to Electromagnetic Radiation. International Patent Application No. AU9948982-A; WO200003589-A1; International Patent Classification: A01M-021/00, 2003.
19. Andreasen, C.; Vlassi, E.; Salehan, N. Laser weeding of common weed species. *Front. Plant Sci.* **2024**, *15*, 1375164. [CrossRef]
20. Andreasen, C.; Vlassi, E.; Salehan, N. Laser weeding: Opportunities and challenges for couch grass (*Elymus repens* (L.) Gould) control. *Sci. Rep.* **2024**, *14*, 11173. [CrossRef]
21. Heisel, T.; Schou, J.; Christensen, S.; Andreasen, C. Cutting weeds with a CO_2 laser. *Weed Res.* **2001**, *41*, 19–29. [CrossRef]
22. Mathiassen, S.K.; Bak, T.; Christensen, S.; Kudsk, P. The effect of laser treatment as a weed control method. *Biosyst. Eng.* **2006**, *95*, 497–505. [CrossRef]
23. Marx, C.; Barcikowski, S.; Hustedt, M.; Haferkamp, H.; Rath, T. Design and application of a weed damage model for laser-based weed control. *Biosyst. Eng.* **2012**, *113*, 148–157. [CrossRef]
24. Zhu, H.; Zhang, Y.; Mu, D.; Bai, L.; Zhuang, H.; Li, H. YOLOX-based blue laser weeding robot in corn field. *Front. Plant Sci.* **2022**, *13*, 1017803. [CrossRef]
25. Hussain, A.; Fatima, H.S.; Zia, S.M.; Hasan, S.; Khurram, M.; Stricker, D.; Afzal, M.Z. Development of cost-effective and easily replicable robust weeding machine—Premiering precision agriculture in Pakistan. *Machines* **2023**, *11*, 287. [CrossRef]
26. Qin, L.; Xu, Z.; Wang, W.; Wu, X. YOLOv7-Based Intelligent Weed Detection and Laser Weeding System Research: Targeting Veronica didyma in Winter Rapeseed Fields. *Agriculture* **2024**, *14*, 910. [CrossRef]
27. Wu, H.; Wang, Y.; Zhao, P.; Qian, M. Small-target weed-detection model based on YOLO-V4 with improved backbone and neck structures. *Precis. Agric.* **2023**, *24*, 2149–2170. [CrossRef]
28. Sandler, M.; Howard, A.; Zhu, M.; Zhmoginov, A.; Chen, L.C. Mobilenetv2: Inverted residuals and linear bottlenecks. In Proceedings of the IEEE Conference on Computer Vision and Pattern Recognition, Salt Lake City, UT, USA, 18–23 June 2018; pp. 4510–4520.
29. Howard, A.; Sandler, M.; Chu, G.; Chen, L.C.; Chen, B.; Tan, M.; Wang, W.; Zhu, Y.; Pang, R.; Vasudevan, V.; et al. Searching for mobilenetv3. In Proceedings of the IEEE/CVF International Conference on Computer Vision, Seoul, Republic of Korea, 27 October–2 November 2019; pp. 1314–1324.
30. Zhang, X.; Zhou, X.; Lin, M.; Sun, J. Shufflenet: An extremely efficient convolutional neural network for mobile devices. In Proceedings of the IEEE Conference on Computer Vision and Pattern Recognition, Salt Lake City, UT, USA, 18–23 June 2018; pp. 6848–6856.
31. Howard, A.G.; Zhu, M.; Chen, B.; Kalenichenko, D.; Wang, W.; Weyand, T.; Andreetto, M.; Adam, H. Mobilenets: Efficient convolutional neural networks for mobile vision applications. *arXiv* **2017**, arXiv:1704.04861.
32. Ma, N.; Zhang, X.; Zheng, H.T.; Sun, J. Shufflenet v2: Practical guidelines for efficient cnn architecture design. In Proceedings of the European Conference on Computer Vision (ECCV), Munich, Germany, 8–14 September 2018; pp. 116–131.
33. Tan, M.; Le, Q. Efficientnet: Rethinking model scaling for convolutional neural networks. In Proceedings of the International Conference on Machine Learning, Long Beach, CA, USA, 9–15 June 2019; pp. 6105–6114.
34. Chen, J.; Kao, S.h.; He, H.; Zhuo, W.; Wen, S.; Lee, C.H.; Chan, S.H.G. Run, don't walk: Chasing higher FLOPS for faster neural networks. In Proceedings of the IEEE/CVF Conference on Computer Vision and Pattern Recognition, Vancouver, BC, Canada, 17–24 June 2023; pp. 12021–12031.
35. Rosenfeld, A.; Pfaltz, J.L. Sequential operations in digital picture processing. *J. ACM* **1966**, *13*, 471–494. [CrossRef]
36. Lumia, R.; Shapiro, L.; Zuniga, O. A new connected components algorithm for virtual memory computers. *Comput. Vision, Graph. Image Process.* **1983**, *22*, 287–300. [CrossRef]
37. Chen, W.; Giger, M.L.; Bick, U. A fuzzy c-means (FCM)-based approach for computerized segmentation of breast lesions in dynamic contrast-enhanced mr images1. *Acad. Radiol.* **2006**, *13*, 63–72. [CrossRef] [PubMed]
38. Ding, M.; Cao, Y.F.; Wu, Q.X. Autonomous craters detection from planetary image. In Proceedings of the 3rd International Conference on Innovative Computing Information and Control, Dalian, China, 18–20 June 2008; p. 443.

39. Abuzaghleh, O.; Barkana, B.D.; Faezipour, M. Noninvasive real-time automated skin lesion analysis system for melanoma early detection and prevention. *IEEE J. Transl. Eng. Health Med.* **2015**, *3*, 4300212. [CrossRef]
40. Lao, W.; Han, J.; De With, P.H. Automatic video-based human motion analyzer for consumer surveillance system. *IEEE Trans. Consum. Electron.* **2009**, *55*, 591–598. [CrossRef]
41. Joshi, K.A.; Thakore, D.G. A survey on moving object detection and tracking in video surveillance system. *Int. J. Soft Comput. Eng.* **2012**, *2*, 44–48.
42. Cheng, H.Y.; Weng, C.C.; Chen, Y.Y. Vehicle detection in aerial surveillance using dynamic Bayesian networks. *IEEE Trans. Image Process.* **2011**, *21*, 2152–2159. [CrossRef] [PubMed]
43. Mohamed, A.A.; Yampolskiy, R.V. An improved LBP algorithm for avatar face recognition. In Proceedings of the XXIII International Symposium on Information, Communication and Automation Technologies, Sarajevo, Bosnia and Herzegovina, 27–29 October 2011; pp. 1–5.
44. Veeranampalayam Sivakumar, A.N.; Li, J.; Scott, S.; Psota, E.J.; Jhala, A.; Luck, J.D.; Shi, Y. Comparison of object detection and patch-based classification deep learning models on mid-to late-season weed detection in UAV imagery. *Remote Sens.* **2020**, *12*, 2136. [CrossRef]
45. Zhang, J.L.; Su, W.H.; Zhang, H.Y.; Peng, Y. SE-YOLOv5x: An optimized model based on transfer learning and visual attention mechanism for identifying and localizing weeds and vegetables. *Agronomy* **2022**, *12*, 2061. [CrossRef]
46. Chen, D.; Lu, Y.; Li, Z.; Young, S. Performance evaluation of deep transfer learning on multi-class identification of common weed species in cotton production systems. *Comput. Electron. Agric.* **2022**, *198*, 107091. [CrossRef]
47. Peng, H.; Li, Z.; Zhou, Z.; Shao, Y. Weed detection in paddy field using an improved RetinaNet network. *Comput. Electron. Agric.* **2022**, *199*, 107179. [CrossRef]
48. Zou, K.; Liao, Q.; Zhang, F.; Che, X.; Zhang, C. A segmentation network for smart weed management in wheat fields. *Comput. Electron. Agric.* **2022**, *202*, 107303. [CrossRef]
49. Hua, J.; Li, X. Weed identification and localization method of laser weeding robot based on deep learning. *J. Tianjin Polytech. Univ.* **2024**, *12*, 1–9.
50. Hu, R.; Su, W.H.; Li, J.L.; Peng, Y. Real-time lettuce-weed localization and weed severity classification based on lightweight YOLO convolutional neural networks for intelligent intra-row weed control. *Comput. Electron. Agric.* **2024**, *226*, 109404. [CrossRef]